1959

Angular velocity measurement using an undamped gyroscope.

Morrow, Charles D.

Monterey, California: U.S. Naval Postgraduate School

ANGULAR VELOCITY MEASUREMENT USING AN UNDAMPED GYROSCOPE

CHARLES D. MORROW

ANGULAR VELOCITY MEASUREMENT USING AN UNDAMPED GYROSCOPE

* * * * *

Charles D. Morrow

ANGULAR VELOCITY MEASUREMENT USING AN UNDAMPED GYROSCOPE

by

Charles D. Morrow
Lieutenant, United States Navy

Submitted in partial fulfillment of the
requirements for the Completion of Course

GUIDED MISSILE CURRICULUM

United States Naval Postgraduate School
Monterey, California

1 9 5 9

ANGULAR VELOCITY MEASUREMENT USING AN UNDAMPED GYROSCOPE

by

Charles D. Morrow

This work is accepted as fulfilling the
thesis requirements for the Completion of Course
GUIDED MISSILE CURRICULUM
United States Naval Postgraduate School

ABSTRACT

Gyroscopes in their various forms have been used as references for moving bodies. This is an investigation of a proposed gyro to be used as an angular velocity detector; the gyro and associated servo to be a component of a computer for application to a missile guidance system. A scheme for using single degree of freedom undamped gyros on individual platforms is described; the gyro characteristics are analysed. A scheme for using the proposed gyro on a stablized platform is analysed.

The writer wishes to express his appreciation for the assistance and advice given him by Professor M. L. Cotton of the U. S. Naval Postgraduate School, Messrs. Glynn Lockewood, and Albert Chanowitz of the Dalmo Victor Engineering Company, and Lieutenant C. R. Watts, United States Navy.

The analysis was accomplished by Charles D. Morrow, Lieutenant, United States Navy during an industrial experience tour of duty with the Dalmo Victor Engineering Company, 1515 Industrial Way, Belmont, California, and Dalmo Victor Research Engineering Laboratory, 462 Jefferson Street, Monterey, California.

TABLE OF CONTENTS

LIST OF ILLUSTRATIONS

1. Introduction

This investigation resulted from a proposal to use a gyroscope as a component of a missile guidance system. The construction of the gyro was to be such that the cost of production would be between that of aircraft gyro instruments and the well known HIG gyro.

Input velocities were to be measured by having the gyro output signal amplified and used to activate a servomotor to drive the platform at a velocity equal in magnitude but opposite in direction to that of the input. The platform velocity would then be used in a computer to compute position from an initial reference.

The Minneapolis-Honeywell Company has done a similar investigation, using the HIG gyro. The Minneapolis-Honeywell Company was primarily concerned with drift. This analysis is an investigation of stability.

2. General Considerations

Angular motion of a missile may be measured by fixing the sensitive (input) axis of three single degree of freedom gyros along the roll, pitch and yaw axes of the missile. The measurements are then made in terms of p,q,and r the angular rate of motion relative to the body axis.

These rates are related to a fixed inertial reference frame by the transformation

$$\begin{array}{l} \text{roll} \\ \text{pitch} \\ \text{yaw} \end{array} \begin{vmatrix} A \\ B \\ C \end{vmatrix} = \begin{vmatrix} 1 & \sin\phi\tan\theta & \cos\phi\tan\theta \\ & \cos\phi & -\sin\phi \\ & \sin\phi\sec\theta & \cos\phi\sec\theta \end{vmatrix} \times \begin{vmatrix} p \\ q \\ r \end{vmatrix} \qquad (1)$$

Either set of angles describe the rotational motion of missile.

It is convenient in the analysis to use velocities referred to inertial space (A,B,C).

The problem may be expressed by $\Delta\omega = \omega_{in} + \omega_p$ for each gyro where $\Delta\omega$ is the net angular velocity to which the gyro is sensitive; ω_{in} the input velocity with respect to inertial space and ω_p the platform rate. The simplified diagram of Fig. 1 shows the physical arrangement of one of the platforms.

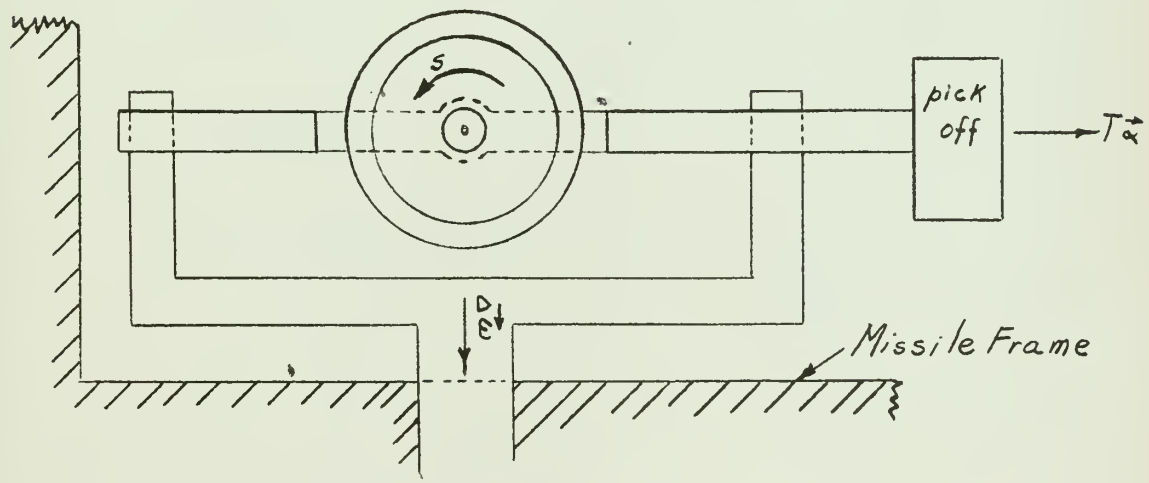

Fig. 1

The direction of the angular displacement of the motor from the null position is best described by the vector cross product.

$$T_{\alpha} = \vec{H} \times \Delta\vec{\omega} \tag{2}$$

The differential equations describing a gyro and its associated servo platform are

$$I_o \ddot{\xi} + D_g \dot{\xi} = \Delta\omega_1 H\cos\xi + \Delta\omega_2 H\sin\xi \tag{3}$$

$$I_p \Delta\dot{\omega}_1 + D_p \omega_{ip} = K_{\xi}\xi + K_{\dot{\xi}}(\dot{\xi} - \Delta\omega_3) H\cos\xi \tag{4}$$

Equation (3) is the sum of torques at the gyro output axis and equation (4) the sum of torques at the platform axis.

The parameters of the system for initial analysis, were estimated to be

I_o = 2000 gm cm^2

D_g = 10 $\frac{\text{dyne cm}}{\text{rad/sec}}$

I_p = 1200 gm cm^2

D_p = 10 $\frac{\text{dyne cm}}{\text{rad/sec}}$

$H = \omega_s I_s = 3\text{x}10^6 \frac{\text{gm cm}^2}{\text{sec}}$

The stable platform system using the same gyro parameters is described by the differential equations

$$I_o \ddot{\xi} + D_g \dot{\xi} = \Delta\omega_i H \cos\alpha \qquad (5)$$

$$I_p \Delta\omega_i + D_p \omega_{ip} = K(\xi \pm \phi_{2p}) \qquad (6)$$

where Ip = 20000 gm cm^2

The last term of equations (3), (4), and (6) are cross coupling terms.

In the configuration of the individual platform system, the gyro is sensitive to components of angular velocity perpendicular to the sensitive axis and the spin axis, while the platform experiences a torque proportional to the net angular rate parallel to the output axis.

In the case of the stable platform the cross-coupling occurs in the pick off, from which the actual signal to be amplified is the sum of angular displacement of the rotor relative to its case and the angular motion of the platform which carries the case, in a direction parallel to the gyro out-put axis.

To simplify the analysis the moments of inertia were considered symetrical so that the cross-products of inertia were negligible.

Coulomb friction which would set the drift sensitivity threshhold to approximately 0.5 degrees per hour was

estimated to be $10 \frac{dyne\ cm}{rad/sec}$. This parameter was neglected in the analysis.

The fact that there are pig-tail electrical leads to the pickoff coils casues a restraint on the gyro rotor. This restraint was included in the gyro analysis.

3. Single Platform System

The block diagram of individual platform system shown in Fig. 2 was arranged to conform to the generalized block diagram shown in Fig. 7. Nodes a through d were added to provide flexibility.

According to the notation of the general signal flow diagram for a 7 node system contained in the Appendix I,

Feed Forward	Feed Back
$G_{aA} = H$	
$G_{bB} = \frac{1}{I_o s}$	$G_{Bb} = Dq$
$G_{cD} = 1$	$G_{Eq} = \cos\alpha$
$G_{dE} = -H\cos\alpha$	$G_{Fe} = Dp$
$G_{ef} = \frac{1}{I_p s}$	
$G_{cE} = \frac{K\alpha}{s} + K\dot{\alpha}$	

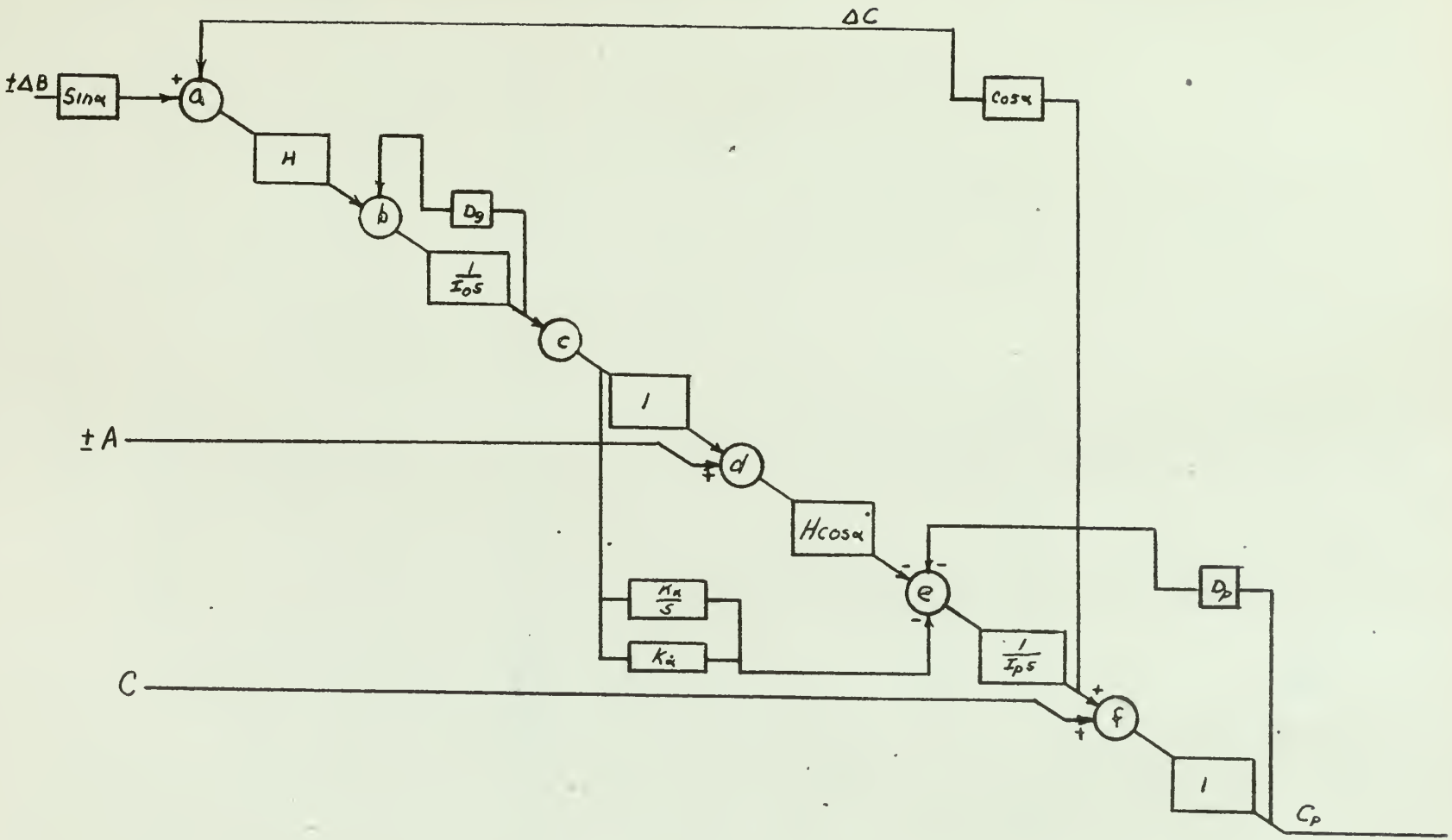

Fig.2 Yaw System

From these factors the determinent Δ was constructed

$$\Delta = \begin{vmatrix} 1 & & & & -\frac{\cos\alpha}{I_p s} & \\ -H & 1+\frac{D_g}{I_o s} & & & & \\ & & 1 & & & \\ & & -1 & 1 & & \\ & & K_\alpha + \frac{K_\alpha}{s} & H\cos\alpha & 1 & D_p \\ & & & & -\frac{1}{I_p s} & 1 \end{vmatrix} \quad (7)$$

from which

$$\Delta = 1 + \frac{D_g D_p + (I_p D_g + I_o D_p)s}{I_p I_o s^2} + \frac{K_\alpha H\cos\alpha + s(K_\alpha H\cos\alpha + H^2\cos^2\alpha)}{I_p I_o s^3} \quad (8)$$

It should be noted that G_{de} and G_{ce} are negative feed forward terms and that G_{eE} is positive feed back, which results in the sign change upon insertion into the determinant.

The terms of Δ are of the form

$$\Delta = 1 + \sum G_{open\ loop}(s) \quad (9)$$

Polar diagrams of each term may be added to obtain a Niquist diagram as a check for stability.

After algebraic manipulation equation (8) becomes

$$\Delta = 1 + \left(\frac{D_g}{I_o} + \frac{D_p}{I_p}\right)\frac{1}{s} + \frac{D_p D_g + K_{\dot{\alpha}} H\cos\alpha + (H\cos\alpha)^2}{I_p I_o s^2} + \frac{K_\alpha H\cos\alpha}{I_p I_o} \qquad (10)$$

upon substitution of numerical quantities

$$\Delta = 1 + 0.01333\left(\frac{1}{s}\right) + \frac{100 + 3\times10^6 K_{\dot{\alpha}}\cos\alpha + 9\times10^{12}\cos^2\alpha}{24\times10^5} + \frac{9\times10^6 K_\alpha\cos\alpha}{24\times10^5} \qquad (11)$$

It was seen that the order of magnitude of the last two terms would cause the first loop function to be insignifigant, if K_α and $K_{\dot{\alpha}}$ were of any great magnitude.

It was estimated that a $\zeta = 0.3$ would be an adequate parameter for fast response. A curve for by Mitrovic's method [10] was constructed to determine values of K_α and $K_{\dot{\alpha}}$. Fig. 3 is the result of the tabulated computations of Table I, from which

$$B_1 = 3.3\times10^{-4} = \frac{100 + 3\times10^6 K_{\dot{\alpha}} + 9\times10^{12}}{2.4\times10^6}$$

$$K_{\dot{\alpha}} = -3\times10^{-6}$$

and

$$B_0 = 9.87\times10^{-6} = \frac{3\times10^6 K_\alpha}{2.4\times10^6}$$

$$K_\alpha = 7.89\times10^{-6}$$

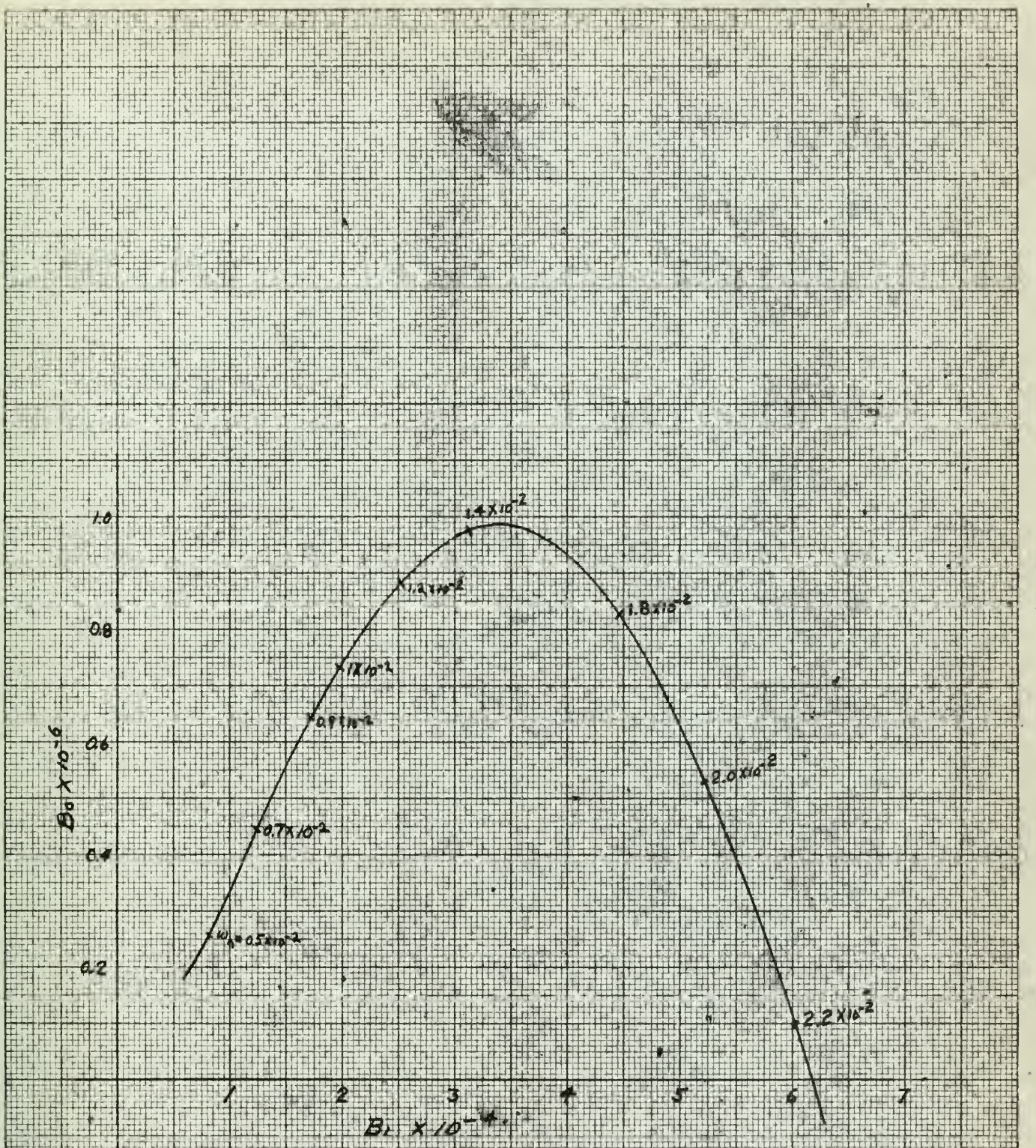

Fig. 3 Mitrovic chart, $\zeta = 0.3$ single platform

9

TABLE I

ω_n	B_o	B_1
0.5×10^{-2}	0.259×10^{-6}	0.806×10^{-4}
0.7×10^{-2}	0.448×10^{-6}	1.247×10^{-4}
0.9×10^{-2}	0.543×10^{-6}	1.718×10^{-4}
1.0×10^{-2}	0.733×10^{-6}	1.970×10^{-4}
1.2×10^{-2}	0.885×10^{-6}	2.522×10^{-4}
1.4×10^{-2}	0.973×10^{-6}	3.121×10^{-4}
1.8×10^{-2}	0.830×10^{-6}	4.470×10^{-4}
2.0×10^{-2}	0.530×10^{-6}	5.226×10^{-4}
2.2×10^{-2}	0.100×10^{-6}	6.025×10^{-4}
2.4×10^{-2}	-0.600×10^{-6}	6.890×10^{-4}

These values were chosen such to take the maximum advantage of amplifier and torque motor gain. It was noted that the system is stable, constrained thus by Mitrovic's method, however to achieve the stability, the sign of the term associated with $K\dot{\alpha}$ must be changed, and that the signal from the angular position pick-off must be attenuated. The changing of sign in the $K\dot{\alpha}$ amplifier would cause the closed loop function to have zeros in the right half of the s-plane. It was observed that the torque associated with the $(H\cos\alpha)^2$ term was a torque caused by cross coupling and that its direction was dependent upon the net rotation of the platform about the gyro output axis, with respect to inertial space.

4. Steady State Response

The steady state response to a step input of velocity was investigated.

The general equation for any input, using the determinant approach [10] is

$$\underset{t\to\infty}{\phi_c(t)_{ss}} = \lim_{s\to 0} s\left(\frac{\Delta_{if}}{\Delta}\right) G(s)_{in}\, G(s)_{out}\, \phi_R(s) \qquad (12)$$

Thus for a step input of velocity at node f , $G(s)_{in}=$ $G(s)_{out} = 1$ and

$$\Delta_{cA} = \begin{vmatrix} 1 & & & & -\frac{\cos\alpha}{I_p s} \\ -H & 1+\frac{D_g}{I_o s} & & & \\ & -\frac{1}{I_o s} & 1 & & \\ & & -1 & 1 & \\ & & K\dot{\alpha}+\frac{K_\alpha}{s} & H\cos\alpha & 1 \\ & & & -\frac{1}{I_p s} & \frac{C}{s} \end{vmatrix} \qquad (13)$$

$$\frac{C_p}{C}(s) = \frac{s^3 + \frac{D_g}{I_o}s^2 + \frac{H\cos\alpha(H\cos\alpha - K\dot{\alpha})}{I_p I_o}s + \frac{K_\alpha H\cos\alpha}{I_p I_o}}{s^3 + \left(\frac{D_g}{I_o}+\frac{D_p}{I_p}\right)s^2 + \frac{D_p D_g + H\cos\alpha(H\cos\alpha - K\dot{\alpha})}{I_p I_o}s + \frac{K_\alpha H\cos\alpha}{I_p I_o}} \qquad (14)$$

$$\lim_{s\to 0} s\,\frac{C_p}{C}(s) \times \frac{1}{s} = 1 \qquad (15)$$

5. Steady State Response to Cross-coupling Inputs

For s unit step input of ΔB at node a

$$\Delta_{aF} = \begin{vmatrix} 1 & & & & -\frac{\cos\alpha}{I_p s} & \frac{\Delta B}{s} \\ -H & 1+\frac{D_g}{I_o s} & & & & \\ & -\frac{1}{I_o s} & 1 & & & \\ & & -1 & 1 & & \\ & & K\dot{\alpha}+\frac{K_\alpha}{s} & H\cos\alpha & 1 & \\ & & & & -\frac{1}{I_p s} & \end{vmatrix} \qquad (16)$$

and

$$C_p(s) = \frac{\Delta B}{s}\left[\frac{\dfrac{H^2 \cos\alpha \sin\alpha\, s^2 + (K_\alpha H \sin\alpha)s + K_\alpha H \sin\alpha}{I_p I_o}}{\Delta}\right] \qquad (17)$$

thus $$\underset{t\to\infty}{C_p(t)} = \underset{s\to 0}{Lim}\; s \times \sin\alpha \frac{C_p}{\Delta B}(s) = \Delta B \alpha$$

for small angles of α .

For a unit step input of A at node d

$$\Delta_{dF} = \begin{vmatrix} 1 & & & & -\frac{\cos\alpha}{I_p s} \\ -H & 1+\frac{D_g}{I_o s} & & & \\ & -\frac{1}{I_o s} & 1 & & \\ & & -1 & 1 & \frac{A}{s} \\ & & K_\alpha + \frac{K_\alpha}{s} & H\cos\alpha & 1 \\ & & & & \frac{1}{I_p s} \end{vmatrix} \qquad (18)$$

$$C_p(s) = \frac{A}{s}\left[\frac{(H\cos\alpha)s^3 + \frac{D_g H\cos\alpha}{I_p I_o}}{\Delta}\right] \tag{19}$$

$$\lim_{t\to\infty} C_p(t) = \lim_{s\to 0} s\,X\,\frac{C_p}{A}(s) = \frac{D_g}{k_\alpha}A \tag{20}$$

By allowing the missile to rotate about all three axes, and assuming linearity of response, the theroem of superposition for outputs at node f may be applied

$$\sum_{t\to\infty} C_p(t) = C \pm \Delta B\alpha \pm \frac{D_g}{k_\alpha}A \tag{21}$$

5. Gyro Performance

The performance of the gyro as a separate unit was analyzed from the sumation of torques at the output axes.

$$T_d = I_o \ddot{\theta} + D_g \dot{\theta} + R\theta \tag{22}$$

$$\frac{\theta}{T_d}(s) = \frac{1/I_o}{s^2 + \frac{D_g}{I_o} s + R}$$

and if an input velocity were the only disturbing torque T_d

$$\frac{\theta}{\omega}(s) = \frac{H/I_o}{\left(s + \frac{D_g}{2I_o}\right)^2 + \left(\sqrt{\frac{R}{I_o} - \left(\frac{D_g}{2I_o}\right)^2}\right)^2}$$

for a step input of velocity

$$\theta(t) = \omega\, 1.5 \times 10^3 \left[20 + 20.15 e^{-0.0025t} \sin(0.2235t - 90.4^\circ)\right] \tag{23}$$

obviously the transient would not die out for a long time.

It was desired to use a position type gyro for these applications. It will be shown, that in the case of the stable element, neither the viscous damping nor the pig-tail restraint affect the stability of this gyro.

The gyro transfer function was

$$\frac{\theta}{\omega}(s) = \frac{H/I_o}{s\left(s + \frac{D_g}{I_o}\right)} \tag{24}$$

Fig. 4 shows the frequency response of the function.

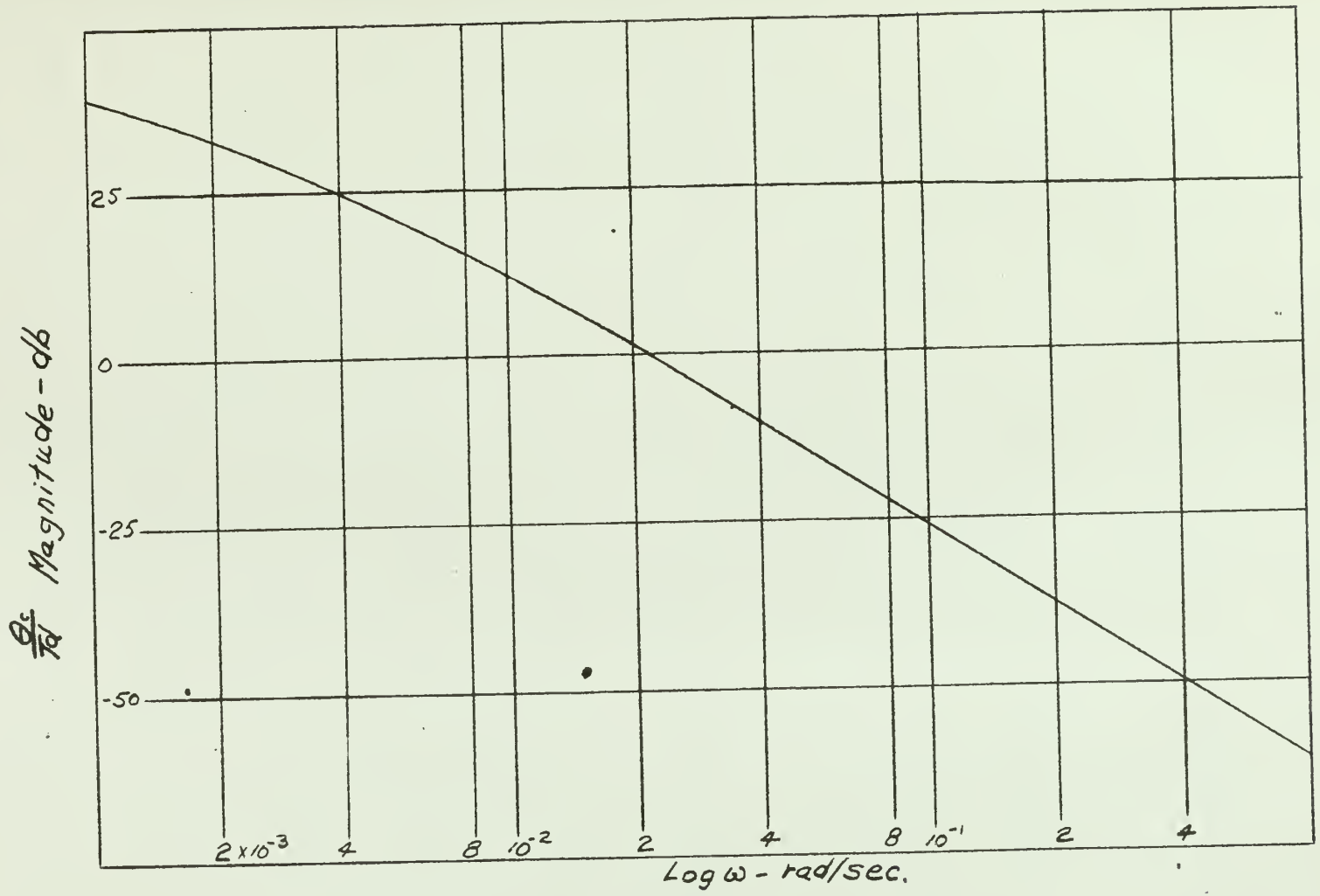

Fig. 4 Gyro frequency response

The transient response to a step input velocity was

$$\theta(t) = \omega \times 3 \times 10^{6} \left[5 \times 10^{-3} t + e^{-0.005t} - 1 \right] \qquad (25)$$

It was noted that in both cases the transient was of extremely long duration, and non-linear.

6. Stable Element

It was decided to investigate a stablized platform configured so as to use the undamped gyro.

Without facilities for simulation of all three degrees of freedom, it proved impractical to obtain an analysis, so only a single degree of freedom with no cross-coupling was considered. Since the gyro was to be mounted on a platform, 20000 dyne-cm^2 was chosen as a representative magnitude of the platform moment of inertia about the inner gimbal axis.

Under the conditions of no cross-coupling and considering only one degree of freedom, the block diagram of the stabilized platform and the single degree of freedom platform are the same, except for the torque caused by the net rotation about the gyro output axis. Cross-coupling in this system occurs in the pick-off due to the motion of the motor element relative to the case, and the case rotating about the output axis due to rotations of the platform about the output axis. Mayer 7 demonstrates that within certain limitations there is an optimum orientation of the gyros for the reduction of oscillation

Fig. 2 represents a dual pick-off stable platform, when the cross-coupling inputs are eliminated and the feed forward path from nodes d to e removed. By so doing node d was eliminated and the system becomes a five node system where

$$\Delta = \begin{vmatrix} 1 & & & -\frac{\cos\alpha}{I_p s} & \\ -H & 1+\frac{D_g}{I_o s} & & & \\ & -\frac{1}{I_o s} & 1 & & \\ & & K_\alpha + \frac{K_\alpha}{s} & 1 & D_p \\ & & & -\frac{1}{I_p s} & 1 \end{vmatrix} \qquad (26)$$

The system shown in Fig. 5, by block diagram reduction had a system function

$$\frac{C_p}{C}(s) = \frac{1}{1+\dfrac{(I_o s^2 + D_g s) D_p}{I_p s (I_o s^2 + D_g s) + H\cos\alpha \left(\dfrac{K_\alpha}{s} + K_\alpha\right)}} \qquad (27)$$

It was seen that this was a unity feed forward system, a fact not obvious when the open loop function was derived by the determinent method. By deleting each one of the pickoffs in turn there are two other possible configurations.

$$\frac{C_p}{C}(s) = \frac{s^3 + \frac{D_g}{I_o} s^2 + \frac{K_\alpha H\cos\alpha}{I_p I_o}}{s^3 + \left(\frac{D_g}{I_o} + \frac{D_p}{I_p}\right) s^2 + \frac{D_p D_g}{I_p I_o} s + \frac{K_\alpha H\cos\alpha}{I_p I_o}} \qquad (28)$$

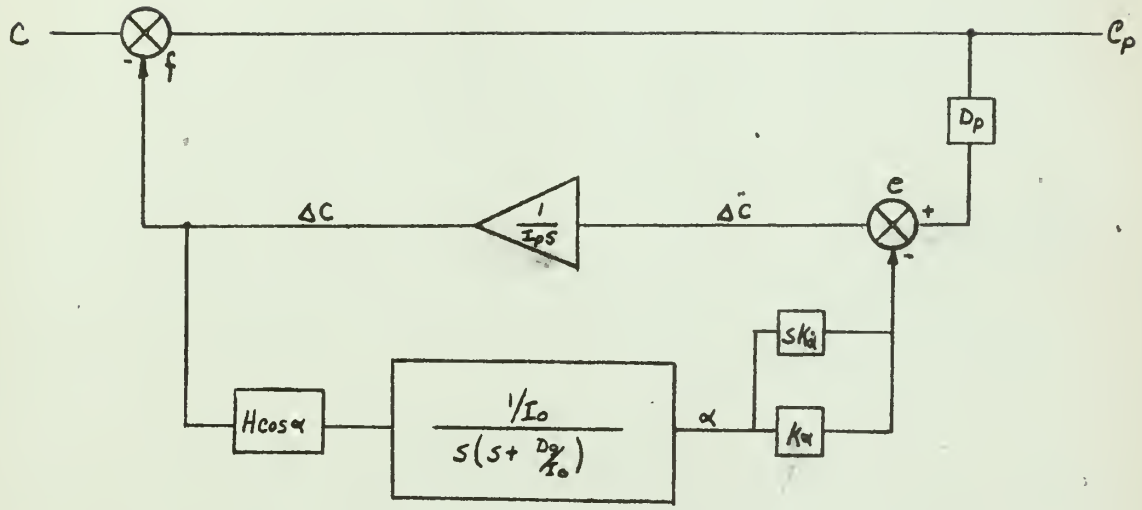

$$\frac{C_p}{C}(s) = \frac{1}{1 + \dfrac{(I_o s^2 + D_g s) D_p}{I_p s \left[I_o s^2 + D_g s + H\cos\alpha (K_{\dot{\alpha}} s + K_\alpha)\right]}}$$

Fig. 5. Yaw System - no cross-coupling

and

$$\frac{C_p}{C}(s) = \frac{s^2 + \frac{D_g}{I_o} s + \frac{K_{\dot{\alpha}} H \cos\alpha}{I_p I_o}}{s^2 + \left(\frac{D_g}{I_o} + \frac{D_p}{I_p}\right) s + \frac{D_g D_p + K_{\dot{\alpha}} H \cos\alpha}{I_p I_o}} \qquad (29)$$

It was considered that the use of the rate pick-off alone would be inadviseable due to the difficulty of measuring the small velocities involved.

The system described by equation (29) is undesireable due to having zeros in the right half of the s-plane. Thus it was chosen to work with the dual pickoff system. Where

$$\frac{C_p}{C}(s) = \frac{s^3 + \frac{D_p}{I_o} s^2 + \frac{H \cos\alpha \left(s K_{\dot{\alpha}} + K_\alpha\right)}{I_p I_o}}{s^3 + \left(\frac{D_g}{I_o} + \frac{D_p}{I_p}\right) s^2 + \frac{D_g D_p + K_{\dot{\alpha}} H \cos\alpha}{I_p I_o} + \frac{K_\alpha H \cos\alpha}{I_p I_o}} \qquad (30)$$

7. Steady State Response

The steady state response to a unit step function of velocity was

$$\lim_{\substack{t \to \infty \\ s \to o}} C_p(t) = s \times \frac{C_p}{C}(s) \times \frac{C}{s} = 1 \qquad (31)$$

8. Stability

A Mitrovic chart, Fig. 6, was made using the characteristic equation of the dual pick-off system. From which

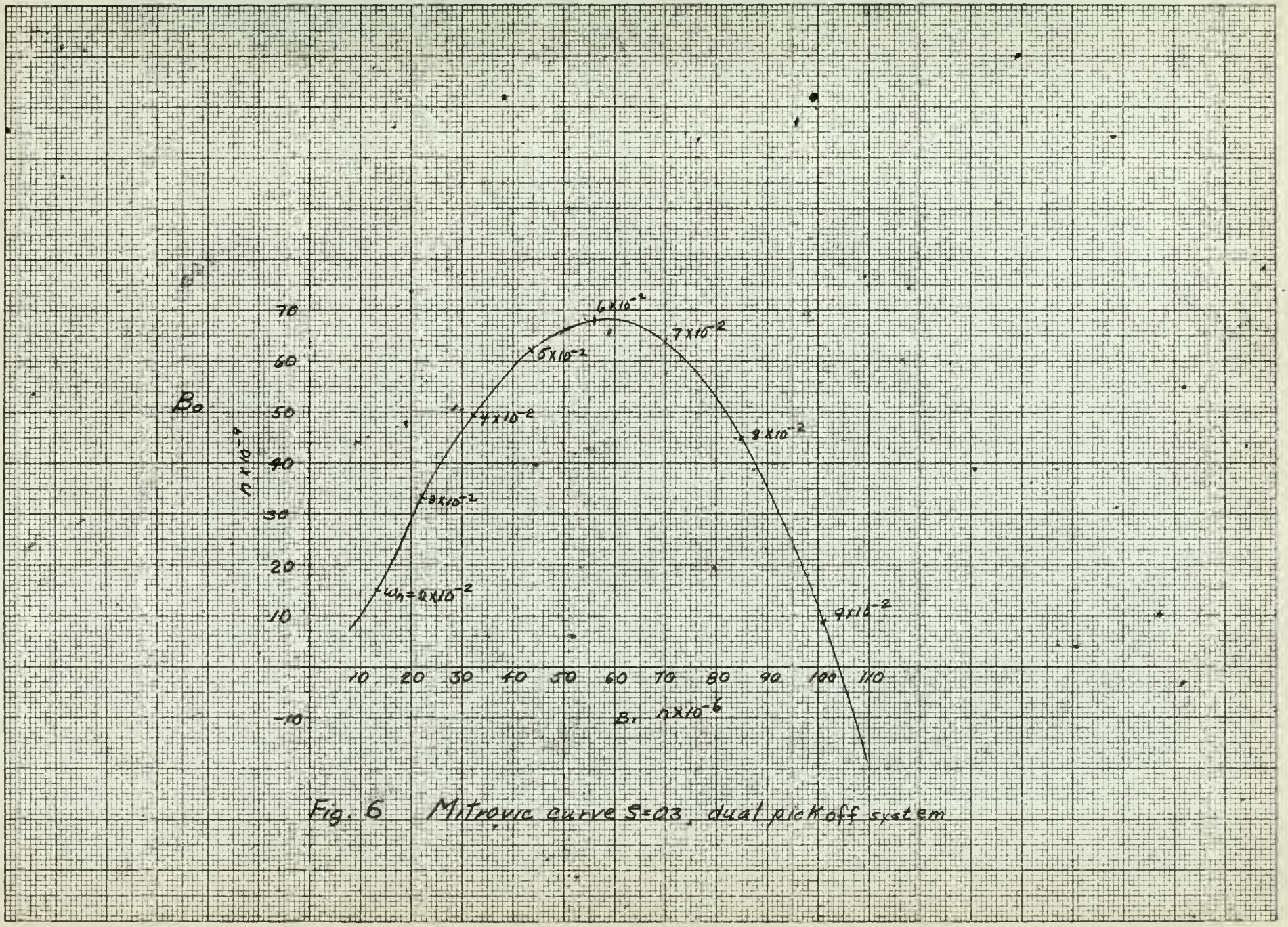

Fig. 6 Mitrovic curve S=03, dual pickoff system

$$K_\alpha = 91.2 \times 10^{-8} \qquad K_{\dot\alpha} = 78 \times 10^{-5}$$

The curve for $\zeta = 0.3$ was chosen on the estimate that it would yield the fastest response.

It was plain that these figures for K_α and $K_{\dot\alpha}$ were unsatisfactory.

By raising the gain of K_α and $K_{\dot\alpha}$ by an amount great enough to make the coefficients of the s^2 term insignifigant and dropping the factor $D_g D_p$ for the same reason the characteristic equation became

$$\Delta = 1 + \frac{K_{\dot\alpha} H}{I_p I_o s^2} + \frac{K_\alpha H}{I_p I_o s^3} \tag{32}$$

for small angles.

The form of the last two terms suggested that the system could use phase lead compensation. A double network of the form

$$G_c(s) = \left(\frac{s\tau + 1}{\frac{s\tau}{3} + 1}\right)^2$$

was chosen, then

$$KG(s) = -1 = \frac{K_\alpha H \left(\frac{K_{\dot\alpha}}{K_\alpha} s + 1\right)(s\tau + 1)^2}{I_p I_o s^3 \left(\frac{s\tau}{3} + 1\right)^2} \tag{33}$$

By choosing $\frac{K_{\dot{\alpha}}}{K_{\alpha}} = \tau$ and using the variable $s\tau$, the open loop function was plotted for unity gain on a Nichols chart, Fig. 7, which showed the system to be stable. A frequency response for $\tau = 1$ and maximum gain of 13 db is shown on Fig. 8.

The high M_p and double peak could probably be eliminated by gain reduction and a change of compensator parameters which would be governed by the application of the system.

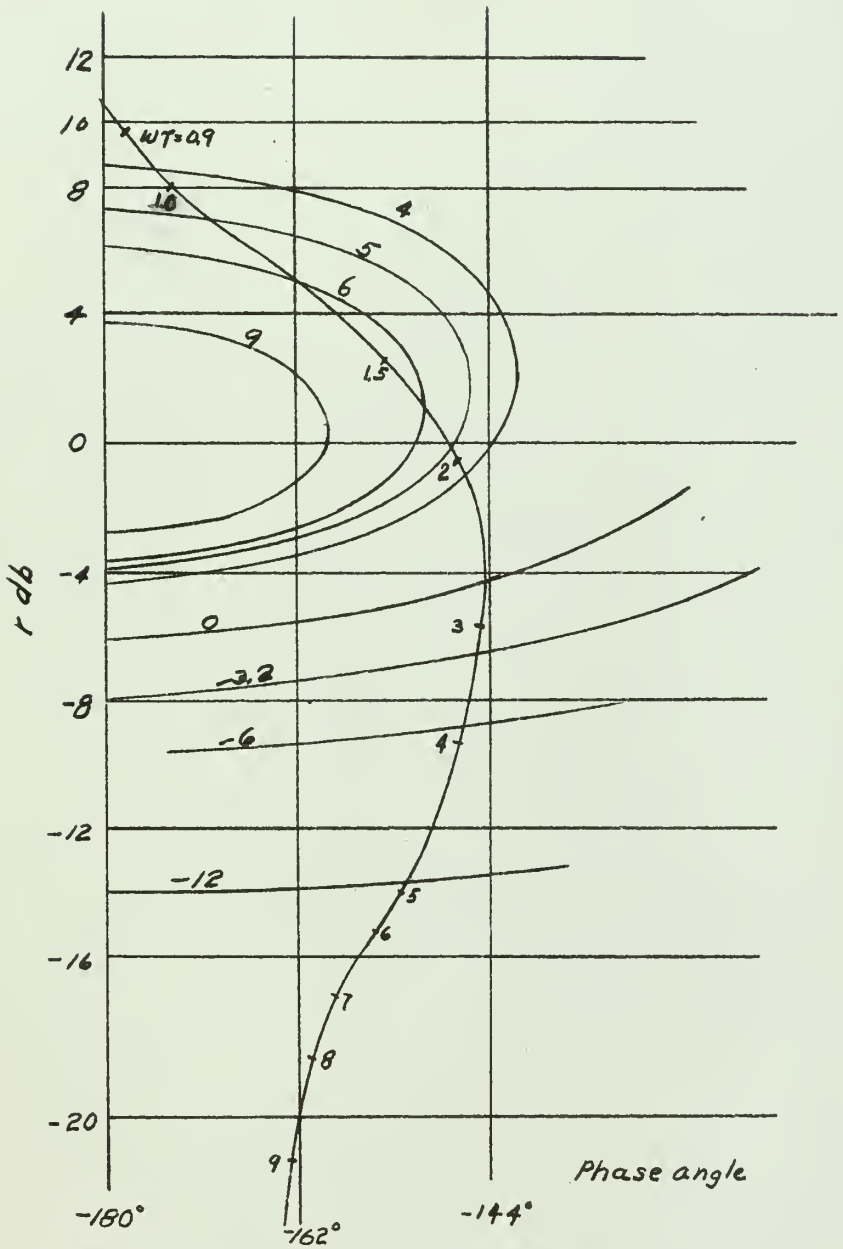

Fig. 7 Nichols Chart for compensated system

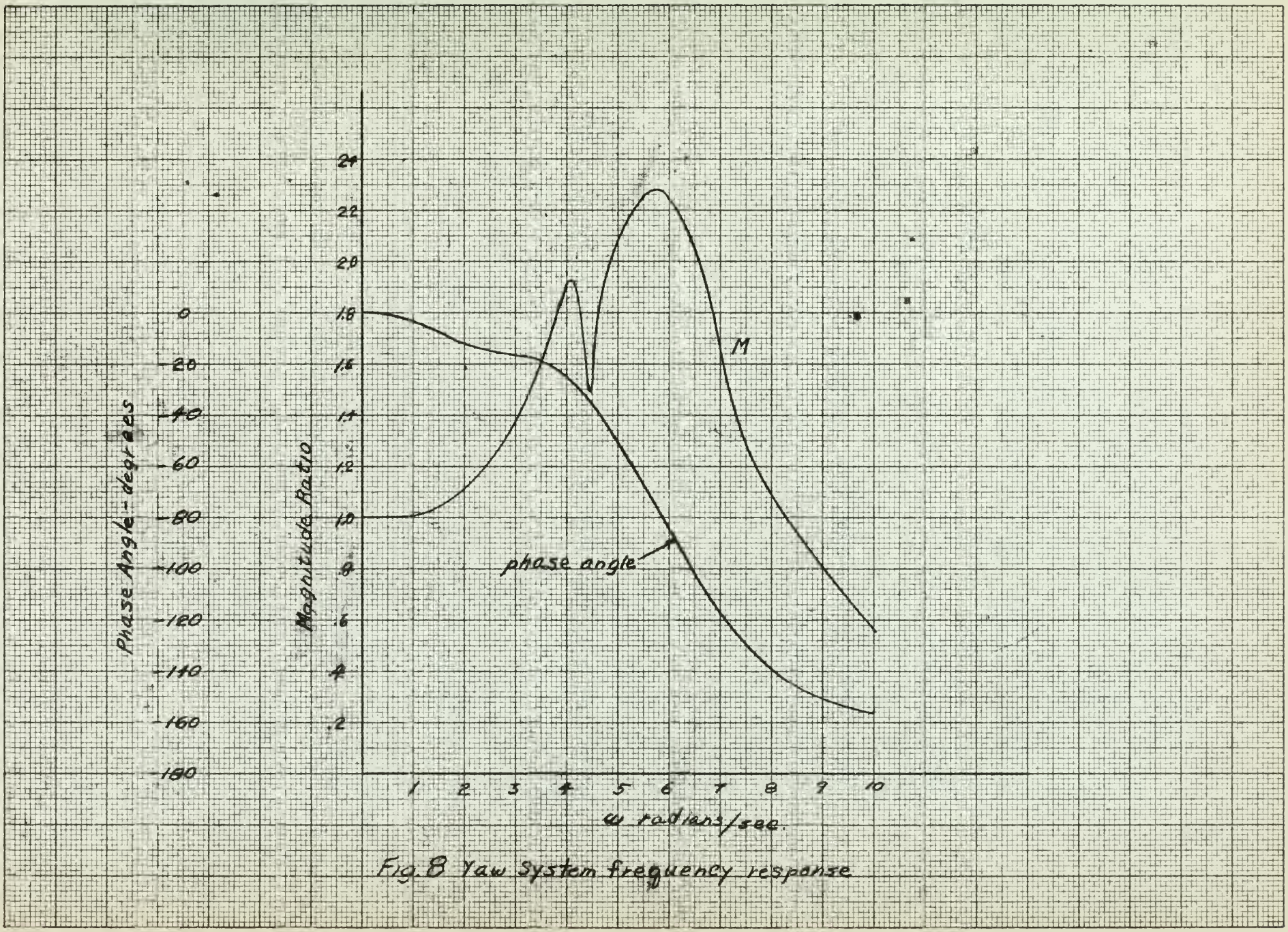

Fig. 8 Yaw System freguency response

9. Results

1. The system of individual platforms will follow all inputs if inputs are maintained long enough. Cross-coupling inputs could be subtracted from any platform motion output in a computer.

2. At low gain the stable element system is conditionally stable.

3. Any gyro drift will be reproduced as a platform motion.

4. The friction damping and pigtail restraint have negligible effect on the stability of the stable element.

5. The gyroscope response is extremely slow.

6. The stable platform, will be stable if the amplifier gain is properly adjusted for the range of frequency of operation.

7. Detecting and amplifying the time rate of change of the gyro precession angle, reduces the requirement for phase lead compensation.

8. The frequency response of the stable element indicates an adequate bandwidth.

9. The frequency response of the gyro indicates large attenuation at the higher frequencies.

10. Conclusions:

1. A greatly increased platform velocity damping would speed up the response of the individual platform system.

2. Increasing the velocity damping of the gyro would improve the linearity of the gyro output and reduce the transient more quickly.

3. There is an advantage to be had by utilizing the time rate of change of precession angle in that less compensation is required to achieve stability.

4. If the attenuation of the gyro output signal at higher frequencies and the non-linearities of the transient can be tolerated the use of the gyro in a stable platform is feasable.

5. The damping of the gyro and platform have little to do with the stability of the inertial platform, but do degrade the form of the gyro output signal.

BIBLIOGRAPHY

1. Richard F. Deimel, Mechanics of the Gyroscope, Dover Publications, inc., 1950.

2. Charles Stark Draper, Walter McKay, Sidney Lees, M.I.T., Instrument Engineering, Vol. I, McGraw-Hill Book Company, Inc., 1952.

3. Kearfott Company, Inc., Gyros, Technical Information for the Engineer, March, 1957.

4. Philip J. Klass, Inertial Guidance, Aviation Week, 1957.

5. Luther Manufacturing Co., Electronic Instrument Components.

6. Jon N. Mangnall, Rigid Body Equations of Motion For Use in Analog Computer Studies of Symmetrical Spinning Missiles, E.A.I. Computation Center, March, 1957.

7. Arthur Mayer, Analysis of Gyro Orientation, I.R.E. Transaction on Automatic Control, Dec., 1958.

8. Floyd E. Nixon, Principles of Automatic Control, Prentice-Hall, Inc., October, 1953.

9. J. B. Scarborough, The Gyroscope, Theory and Application, Interscience Publishers, Inc., 1958.

10. George J. Thaler, Advanced Linear and Nonlinear Compensation Theory, U.S. Naval Postgraduate School, 1958.

11. George J. Thaler, Advanced Linear Servomechanism Theory, U.S. Naval Postgraduate School, 1957.

12. John G. Truxal, Automatic Feedback Control System Synthesis, McGraw-Hill Book Company, Inc., 1955.

13. Walter Wrigley, Roger B. Woodbury, John Hovorka, Inertial Guidance, M.I.T., 1957.

14. C. R. Wylie, Jr., Advanced Engineering Mathematics, McGraw-Hill Book Company, Inc.k 1951.

15. K. I. T. Richardson, The Gyroscope Applied, Hutchinsons Scientific and Technical Publications, Cheltenham Press Ltd., London, 1954.

16. T. Mitsutomi, Characteristics and Stabilization of an Inertical Platform, IRE Transactions on Aeronautical and Navigational Electronics, Vol. ANE 5, June 1958.

APPENDIX I

The characteristic equation was developed by arranging the system to conform to the general block diagram and setting up an array

	a	b	c	d	e
A	$1+G_{ab}G_{Aa}$	$G_{bc}G_{Ba}$			
B	$-G_{ab}$	$1+G_{bc}G_{Bb}$	Feed-back terms		
C	$-G_{ac}$	$-G_{bc}$	$1+G_{cd}G_{Cc}$		
D	Feed-forward terms			-	
E					$1+G_{ef}G_{Ee}$

(1)

The numerator of the closed loop function is the product $\mathcal{L}\, C(s)\, \Delta_{ij}$ where Δ_{ij} is the minor of the column i associated with the input node and j is the row associated with the desired output node.

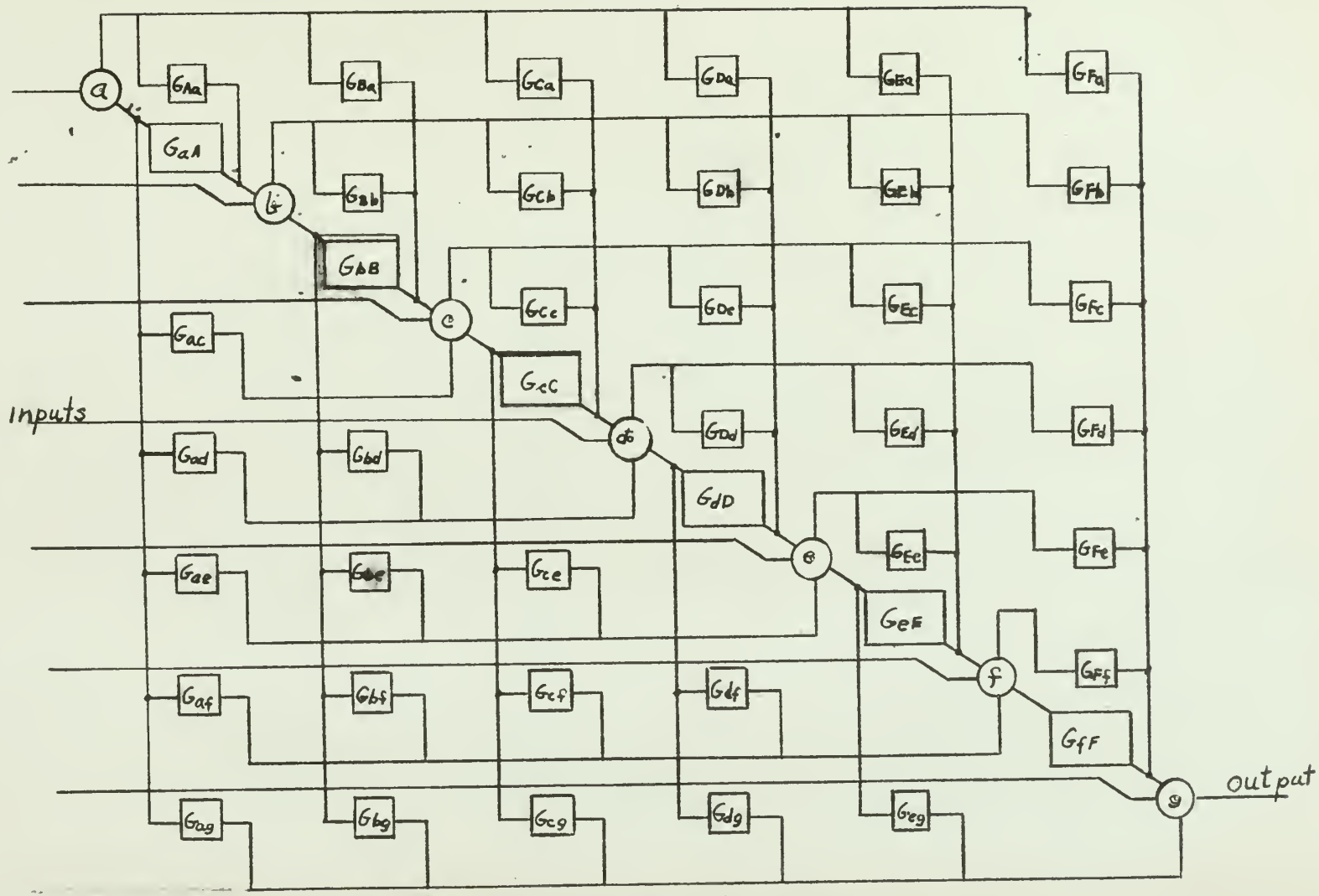

Fig. 9 General Block Diagram

APPENDIX II

The Mitrovic method curves [10] were obtained from the generalized equation:

$$\Delta = a_n s^n + - - - - - - - - - - - + a_1 s + a_0 \qquad (1)$$

Let $\quad s = -\zeta\omega_n + j\omega_n\sqrt{1-\zeta^2}$

After substitution (1) may be written as two simultaneous equations since the summation of reals and imaginaries must go to zero independently, then

Let $B_1 = a_1$, $B_0 = a_0$

$$B_0 = -\omega_n^2\left[a_2\phi_1(\zeta) + a_3\omega_n\phi_2(\zeta) - - - + a_n\omega_n^{n-2}\phi_{n-1}(\zeta)\right] \qquad (2)$$

$$B_1 = a_2\omega_n\phi_2(\zeta) + a_3\omega_n^2\phi_3(\zeta) - - - - + a_n\omega^{n-1}\phi_n(\zeta) \qquad (3)$$

$$\phi_n(\zeta) = -2\zeta\phi_{n-1}(\zeta) + \phi_{n-2}(\zeta) \qquad n \geq 2 \qquad (4)$$

The location of point M at coordinates (B_1B_0) enclosed by the $\zeta = 0$ curve define stability limits.

LIST OF SYMBOLS

1.	ξ, θ	Gyro angle output
2.	$\omega_{1,2,3}$	Velocity along three orthogonal axes
3.	ϕ_{2p}	Angular position with respect to inertial space of a platform, in the direction of the gyro output axis.
4.	Td	Disturbance torque
5.	R	Restraint on gyro caused by electrical leads